J Biomol NMR (2013) 57:91–102
DOI 10.1007/s10858-013-9766-2

ARTICLE

Determination of structural topology of a membrane protein in lipid bilayers using polarization optimized experiments (POE) for static and MAS solid state NMR spectroscopy

Kaustubh R. Mote · T. Gopinath · Gianluigi Veglia

Received: 19 December 2012 / Accepted: 26 July 2013 / Published online: 21 August 2013
© Springer Science+Business Media Dordrecht 2013

Abstract The low sensitivity inherent to both the static and magic angle spinning techniques of solid-state NMR (ssNMR) spectroscopy has thus far limited the routine application of multidimensional experiments to determine the structure of membrane proteins in lipid bilayers. Here, we demonstrate the advantage of using a recently developed class of experiments, polarization optimized experiments, for both static and MAS spectroscopy to achieve higher sensitivity and substantial time-savings for 2D and 3D experiments. We used sarcolipin, a single pass membrane protein, reconstituted in oriented bicelles (for oriented ssNMR) and multilamellar vesicles (for MAS ssNMR) as a benchmark. The restraints derived by these experiments are then combined into a hybrid energy function to allow simultaneous determination of structure and topology. The resulting structural ensemble converged to a helical conformation with a backbone RMSD $\sim$0.44 Å, a tilt angle of 24° $\pm$ 1°, and an azimuthal angle of 55° $\pm$ 6°. This work represents a crucial first step toward obtaining high-resolution structures of large membrane proteins using combined multidimensional oriented solid-state NMR and magic angle spinning solid-state NMR.

Keywords Oriented solid-state NMR (OSS-NMR) · Magic angle spinning solid state NMR · Membrane proteins · DUMAS-ssNMR · MEIOSIS · Sarcolipin · Magnetically aligned bicelles · Hybrid method for membrane protein structure determination

Abbreviations

SLN	Sarcolipin
SERCA	Sarcoplasmic reticulum Ca^{2+}-ATPase
DMPC	1,2-Dimyristoyl-sn-glycero-3-phosphocholine
D6PC	1,2-Dihexanoyl-sn-glycero-3-phosphocholine
POPC	1-Palmitoyl, 2-oleyl-sn-glycero-3-phosphocholine
PISA	Polarity index slant angle
DUMAS	Dual acquisition magic angle spinning
MEIOSIS	Multiple Experiments via Orphan Spin Operators

Introduction

Membrane protein function is modulated by lipid membranes (Tamm 2005; White 2009). Therefore, understanding the structure–function relationship of these proteins requires their characterization in hydrated lipid bilayers. Multidimensional solid-state NMR, i.e. oriented solid-state NMR (O-ssNMR) and magic angle spinning solid-state NMR (MAS-ssNMR), allows for such structural characterization in the presence of fluid lipid bilayers—the most faithful mimetic of natural membranes. O-ssNMR provides information on dipolar couplings and anisotropic chemical shifts that enable the determination of topological parameters, such as the tilt and rotation angles of transmembrane and membrane anchored domains (Veglia et al. 2012). On

Electronic supplementary material The online version of this article (doi:10.1007/s10858-013-9766-2) contains supplementary material, which is available to authorized users.

K. R. Mote · G. Veglia
Department of Chemistry, University of Minnesota, Minneapolis, MN 55455, USA

T. Gopinath · G. Veglia (✉)
Department of Biochemistry, Molecular Biology and Biophysics, University of Minnesota, 207 Pleasant St. S.E., Minneapolis, MN 55455, USA
e-mail: vegli001@umn.edu

the other hand, MAS-ssNMR provides chemical shift information on both main chain and side chains that can be converted into torsion angles for assessing secondary structure elements. MAS-ssNMR can also be utilized to measure residual dipolar couplings in aligned bicelles (Canlas et al. 2008). In the case of fast uniaxial rotation around membrane normal, MAS-ssNMR can provide orientational restraints that can further refine the structure of small peptides (Hu et al. 2010) as well as large membrane proteins (Park et al. 2012; Das et al. 2012).

As we demonstrated for phospholamban (Traaseth et al. 2009; Verardi et al. 2011), the ab initio determination of the structural topology of a membrane protein in the absence of homology models entails the combination of all of the above information. Lack of information or even relying on only one approach to determine the structural topology of membrane proteins leads to misinterpretation of the experimental results (Traaseth et al. 2007; Shi et al. 2011b).

A major advantage of combining MAS-ssNMR and O-ssNMR is that the structural and topological data are obtained using similar lipid compositions, circumventing the necessity for cross-validation of the structural information obtained from different membrane mimetic systems. Nonetheless, the ssNMR experiments applied to membrane proteins are inherently insensitive. This is due in part to the need for high lipid-to-protein ratios that, while maintaining protein's functional integrity, reduce the effective protein concentration in the sample. In addition, recurring secondary structure elements (multiple transmembrane α helices) as well as sample heterogeneity tend to give poorly resolved spectra for these proteins. As a result only a few structures of membrane proteins have been determined by ssNMR techniques (Ketchem et al. 1993; Traaseth et al. 2009; Cady et al. 2009; Sharma et al. 2010; Park et al. 2010; Verardi et al. 2011). Our work is motivated by the necessity of improving these techniques for membrane protein samples. Toward this goal, we recently designed several new pulse sequences to improve the sensitivity of both O-ssNMR and MAS-ssNMR experiments. An underlining concept for these new experiments is the *optimization of nuclear spin polarization* [polarization optimized experiments (POE)] to augment the NMR signals or deconvolute multiple excitation pathways to obtain several 2D or 3D experiments simultaneously. The latter translates into a substantial decrease in experimental time.

For O-ssNMR, the polarization is optimized by recovering the previously discarded dipolar (Gopinath and Veglia 2009) and chemical shift coherences (Gopinath et al. 2010a). We demonstrated that these experiments improve the sensitivity of traditional rotating frame SLF experiments such as PISEMA (Wu et al. 1994), HIMSELF (Dvinskikh et al. 2006), SAMPI-4 (Nevzorov and Opella 2003) and HETCOR (Maudsley and Ernst 1977) by ~40 %, thereby cutting experimental time in half (Gopinath et al. 2010a; b). Such a strategy has also been demonstrated for the PELF experiment (Schmidt-Rohr et al. 1994), and enhances sensitivity by >100 % for highly mobile segments in proteins (Gopinath et al. 2011). The gain in sensitivity has allowed us to record comparatively insensitive constant-time experiments, such as the SECT-PISEMA (Gopinath and Veglia 2010) for increasing resolution in 2-dimensional experiments (Mote et al. 2011). In the 3D SE-PISEMAI-HETCOR experiment (Gopinath et al. 2010a), we designed a pulse scheme to recover chemical shift coherences in addition to retaining the sensitivity gain obtained by the polarization inversion. The resulting boost in sensitivity is 80–180 %, which enables the implementation of 3D spectroscopy to correlate ^{15}N chemical shifts, ^{15}N-^{1}H dipolar couplings, and ^{1}H chemical shifts. The threefold to sevenfold savings in time alone bring a number of membrane protein systems within reach of this technique. This experiment is used here to obtain the complete set of backbone orientation restraints for sarcolipin in oriented bicelles (Dürr et al. 2012).

In contrast to O-ssNMR, MAS-ssNMR experiments have reached a much higher level of sophistication. In the past decade, many groups have used MAS to for high-resolution structural studies of macromolecular systems, including microcrystalline proteins (Castellani et al. 2002; Wylie et al. 2011; Knight et al. 2012), fibrillar systems (Loquet et al. 2012), membrane proteins (Shi et al. 2011a; Tang et al. 2011), protein complexes (Nieuwkoop and Rienstra 2010), cell extracts (Miao et al. 2012) and whole cell (Renault et al. 2012b). Nonetheless, membrane protein structural biology still offers the biggest challenge for MAS techniques, due to dynamic and static disorder that broaden the resonances of ^{13}C and ^{15}N spectra. Various approaches have been devised to overcome these hurdles: faster spinning rates (Demers et al. 2011), extensive (Reif 2012) and partial deuteration (Asami et al. 2012) coupled with ^{1}H detection (Reif et al. 2001; Zhou et al. 2012; Marchetti et al. 2012), sparse ^{13}C labeling to reduce spectral complexity (Sperling et al. 2010) and minimize ^{13}C-^{13}C couplings as a source of line-broadening (Loquet et al. 2011) as well as the use of techniques such as RELOAD (Lopez et al. 2009) to gain sensitivity. One can boost sensitivity to an even higher degree by dynamic nuclear polarization (Hall et al. 1997), opening up this technique to even bigger systems (Renault et al. 2012a).

All of the above experiments, however, do not take full advantage of the sparse nuclear spin polarization. To address this issue, we introduced the Dual-Acquisition MAS strategy (DUMAS) (Gopinath and Veglia 2012a). This novel strategy allows the concatenation of 2D or 3D pulse sequences into a single experiment and it is compatible with all the aforementioned advances, boosting the

capacity of any NMR spectrometer at least twofold without the need for sample manipulation or additional hardware. At the heart of this approach is simultaneous cross-polarization from ^{1}H to ^{13}C and ^{15}N, which has also been used in time-shared experiments (Linser et al. 2011; Nielsen et al. 2012), and long lived ^{15}N longitudinal magnetization (Giraud et al. 2005) which can be stored and recalled to perform additional experiments. The DUMAS scheme enables one to acquire two experiments: the first with 100 % of the sensitivity with respect to classical pulse sequences, and a second experiment generated from the ^{15}N polarization with typically 80 % of the sensitivity (Gopinath and Veglia 2012a). A well-designed combination of these experiments allows sequential assignment as well as side chain assignment in a single 3D experiment (Gopinath and Veglia 2012b). Using the initial scheme of the DUMAS experiments, it is possible to decode the coherences in multidimensional NMR experiments to recover the orphan spin operators that are discarded from the classical experiments. This approach that we called MEIOSIS (Multiple Experiments via Orphan SpIn operatorS) enables one to collect up to four multidimensional NMR experiments with a time saving greater than 50 % (Gopinath and Veglia 2013). See Supplementary Tables 1–3 and Fig S5 and S6 for a detailed comparison of time savings using different sequences on SLN.

In this article, we use POE both in O-ssNMR and MAS spectroscopy to determine the structural topology of sarcolipin, a 3.8 kDa single transmembrane regulator of the sarco(endo)plasmic reticulum Ca^{2+}-ATPase (SERCA) (Odermatt et al. 1998; Traaseth et al. 2008). The traditional approach to solve membrane protein structure by ssNMR would involve the following experimental steps before structure calculation: (a) Obtaining preliminary 2D spectra to optimize elements in the pulse sequence such as DARR mixing times, indirect evolution times as well as the determining the relative sensitivity and resolution attainable in each dimension, (b) Obtaining 3D experiments based on the knowledge gained from the 2D experiments to sequentially assign the protein and (c) complementing these secondary structure restraints obtained from MAS-ssNMR with orientation restraints on the backbone amide residues from O-ssNMR. We show the utility of DUMAS and MEIOSIS in combining multiple experiments to reduce experimental time, so one can simultaneously optimize mixing times, indirect evolution times as well as make decisions about which 3D experiments have the best chance of giving a complete sequential assignment. We also show the use of complementary 3D experiments simultaneously acquired to sequentially assign the protein. Finally we show the tremendous time savings that can be obtained by using the sensitivity enhanced versions of 3D O-ssNMR pulse sequences which give the complete set of orientation restraints on the protein backbone, viz. ^{15}N and ^{1}H anisotropic chemical shifts and ^{15}N-^{1}H dipolar couplings. The individual restraints (anisotropic and isotropic) obtained exclusively by these solid state NMR approaches are then combined in a manner analogous to the previously described hybrid approach (Shi et al. 2009b; Veglia et al. 2012) using an improved algorithm to converge to a structure ensemble with sub-angstrom precision.

Experimental methods

Protein expression, purification and sample preparation

SLN was over-expressed in *E. coli* bacteria fused to a maltose binding protein (MBP), cleaved, and purified as described earlier (Buck et al. 2003; Veglia et al. 2010). Recombinant SLN was purified using reverse-phase HPLC. The fractions containing the protein were lyophilized and used for all solid state NMR experiments. The protein concentration was assessed using UV spectrophotometry using absorption at 280 nm ($\varepsilon = 10{,}300\ M^{-1}\ cm^{-1}$) as well as SDS-PAGE gels using densitometry. For the bicelle preparations, approximately 3.5 mg SLN was dissolved in 6.7 mg D6PC in 20 mM HEPES/100 mM NaCl buffer at pH 7.0 and then added to 31 mg 4:1 DMPC/POPC vesicles suspension. After several freeze thaw cycles, the bicellar phases were formed and transferred to a cylindrical sample holder. For MAS preparations, 2.2 mg of uniformly-[^{13}C,^{15}N]-SLN was reconstituted in DPC micelles and added to 15 mg deuterated DMPC lipids dissolved in DPC micelles. The detergent was removed by incubating the solution with Biobeads SM2 (30:1 ratio with the detergent) for 3 h at room temperature. The protein-lipid vesicles were collected as a pellet by centrifugation at 200,000×*g* at 4 °C for 1 h and packed in a 3.2 mm MAS rotor for NMR experiments without further treatment.

NMR spectroscopy

O-ssNMR experiments

Experiments on bicelle preparations were carried out on a 16.85T VNMRS Spectrometer with a low-E bicelle probe built by the RF Program at NHMFL, Tallahassee, FL (Gor'kov et al. 2007). Temperature was maintained constant at 298.15 K and bicelle alignment was confirmed by a ^{31}P spectrum. After initial optimization (Fig S1), the 3D-SE-PISEMAI-HETCOR experiment (Fig. 1a) was performed with 80 transients for each of the 20 t_1 (^{1}H-^{15}N-DC dimension, evolution time of 2.4 ms) and 15 t_2 (^{1}H-CS dimension, evolution time of 1.13 ms). A cross

polarization time of 1,000 μs, direct dimension acquisition time of 5 ms, and a recycle delay of 3 s were used in all experiments. A 50–70 Hz Lorentz-to-Gauss apodization was used in the direct dimension and a 100 Hz Gaussian apodization was used in the indirect dimensions. The matrix size before Fourier transformation was 8,192 × 256 × 256.

MAS-ssNMR experiments

MAS experiments on SLN in lipid vesicles were carried out on either a 14.09T or a 16.85T VNMRS Spectrometer with a 3.2 mm BioMAS^{TM} probe (Agilent Technologies) at a spinning speed of 10.0 kHz and a temperature of 277.15 K. Two-dimensional MAS-ssNMR experiments were carried out by combining ^{13}C-^{13}C DARR, CA(N)CO, NCO and N(CA)CX experiments into a single 2D experiment using the MEIOSIS (Multiple Experiments via Orphan Spin Operators) strategy (Fig. 1b) (Gopinath and Veglia 2013). Simultaneous cross-polarization from ^{1}H to ^{13}C and ^{15}N was obtained using a contact time of 300 μs, with the RF power of ^{15}N and ^{13}C channels set to 35 kHz and ^{1}H RF power optimized to achieve the n = 2 side-band matching condition (59 kHz). The phase of ^{15}N spinlock during NCA transfer is altered between +x and −x and the resultant data is stored in separate files. Sum and difference of the two data sets with phases x and −x respectively gives DARR and N(CA)CX for the first acquisition, and NCO and CA(N)CO for the second acquisition. Fig S3 and Fig S4 show the dependence of the contact time for the first SPECIFIC-CP step on the distribution of polarization amongst different pathways. It was found that 3,000 μs was the optimal contact time, as it gave the maximum NCα transfer for both N(CA)CX and CA(N)CO experiments. As with a microcrystalline preparation of ubiquitin (Gopinath and Veglia 2013), we found that at this contact time, 54 % residual polarization is left on ^{13}C (to be used for a ^{13}C-^{13}C DARR experiment) and 34 % residual polarization is left on ^{15}N (to be used for a NCO experiment).

The ^{13}C-edited experiments (DARR and CA(N)CO) were acquired with a dwell time of 32 μs for 128 indirect points (t1 evolution of 4.096 ms) while the ^{15}N-edited experiments were acquired with a dwell time of 320 μs for 16 indirect points (t1 evolution of 4.8 ms). Acquisition

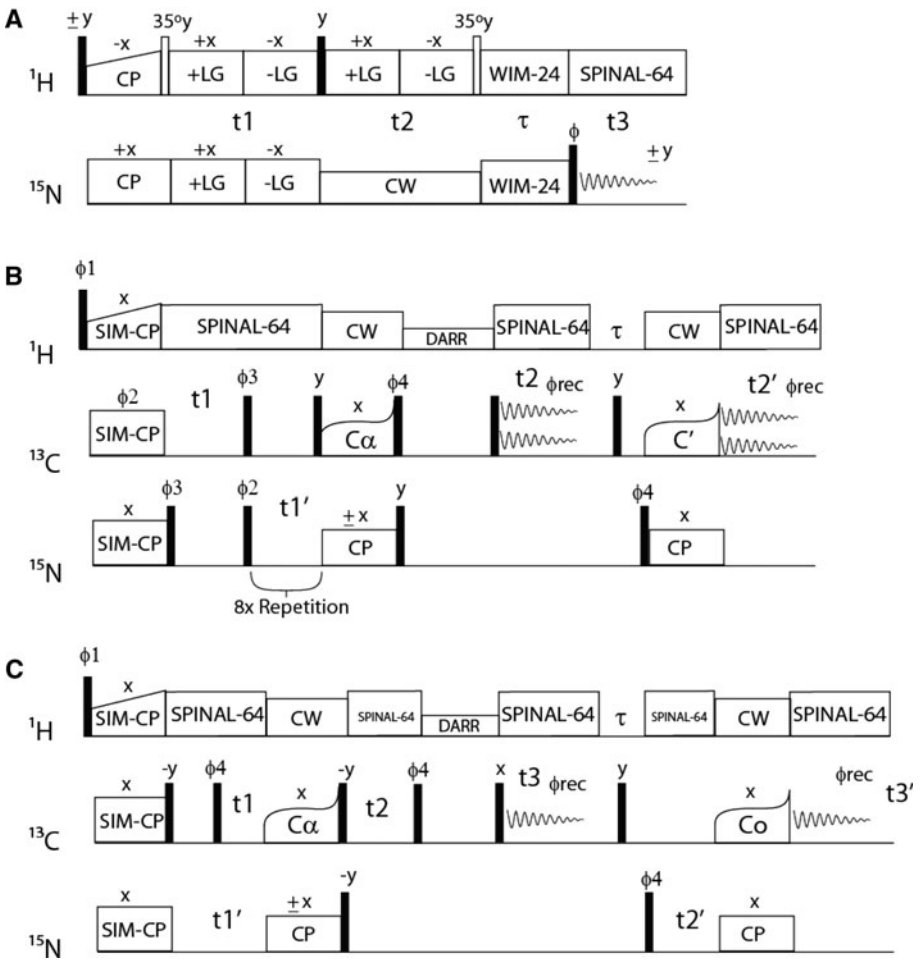

Fig. 1 Pulse sequences O-ssNMR and MAS-ssNMR experiments. **a** SE-PISEMAI-HETCOR, **b** 2D-MEIOSIS-(DARR/N(CA)CX/CA(N)CO/NCO) with the following phases: ϕ1 = {y y y y −y −y −y −y}, ϕ2 = {x x −x −x}$_2$, ϕ3 = {y −y y −y}$_2$, ϕ4 = {y y −y −y}, ϕrec = {x −x −x x −x x x −x} and **c** 3D-DUMAS(CANCO/NCACX) with the following phases: ϕ1 = (y, −y)$_4$, ϕ2 = (y, y, y, y, −y, −y, −y, −y), ϕ3 = (x, x, −x, −x)$_2$, ϕrec = (x, −x, −x, x, −x, x, x, −x). For the pulse sequence in **b**, the ^{13}C carrier frequency is placed in the center of the spectral window for DARR (100 ppm). SPECIFIC-CP is achieved by a phase modulated pulse on ^{13}C that effectively changes the offset to ^{13}Cα (64 ppm) for the first transfer and to C′ (178 ppm) for the second transfer

time of 15 ms and recycle delay of 2 s was used. 64 transients were used for each t1 increment. Due to the reduced spectral width in the ^{15}N dimension, the ^{15}N-edited experiments can be acquired eight times along with a single acquisition of ^{13}C-edited experiments. The number of transients for the NCO and N(CA)CX experiments thus becomes 512 (64 × 8). We acquired two independent experiments at the mixing times of 10 and 50 ms during the DARR transfer. As this transfer does not affect the NCO and CA(N)CO experiments, a further boost in sensitivity is obtained by adding these experiments, giving the total number of transients for NCO and CA(N)CO as 1,024 and 128, respectively. As these are the least sensitive amongst the four concatenated experiments (Fig S3), this design allowed us to boost its sensitivity by repetition, even while optimizing the other experiments. Thus, in the end, we had a total of 6 spectra from 2 separate experiments—^{13}C-^{13}C DARR with 2 different mixing times (with 64 transients each), N(CA)CX with 2 different mixing times (with 512 transients each), CA(N)CO (128 transients) and NCO (1,024 transients). Note that the traditional approach would have allowed the recording of only 2 of these 6 experiments in the same time. For more details on the setup of DUMAS and MEIOSIS experiments and how these experiments can be tailored to suit any given sample, the reader is referred to supplementary information accompanying this article.

3D-DUMAS-ssNMR

To assign the backbone and side chain atoms, we performed the 3D-DUMAS-NCACX-CANCO experiment (Fig. 1c) at 277.15 K and 10.0 kHz MAS spinning. The t1 dimensions for both experiments were co-evolved with a dwell time of 150 μs for the ^{13}C-dimension (CANCO) and 300 μs for the ^{15}N-dimension (NCACX). 16 t1 points were obtained, giving a total of 2.4 ms evolution for ^{13}C and 4.8 ms evolution for ^{15}N respectively. Bidirectional SPECIFIC-CP (Gopinath and Veglia 2012b) from ^{13}Cα to ^{15}N (CANCO) and ^{15}N to ^{13}Cα (NCACX) was achieved with a contact time of 3 ms at RF field strength of 25 kHz (5.ω_r/2) on ^{15}N, and a ^{13}C RF amplitude of 15 (3.ω_r/2) and 35 (7.ω_r/2) kHz for Cα and CO transfer respectively.^{15}N magnetization was stored along the z-direction with a 90° pulse after the t1 evolution periods. ^{13}C-dimension (NCACX) was then evolved, followed by a 10 ms DARR mixing period and finally detected (NCACX) with a 20 ms acquisition time. After this acquisition, the ^{15}N magnetization was brought to the transverse plane with another 90° pulse and evolved (CANCO). Magnetization was then transferred to ^{13}CO with a 3 ms contact time. The second detection of the ^{13}C dimension (CANCO) was again carried out with an acquisition time of 20 ms. The t2 dimensions were thus evolved independently for both experiments with 16 points each, giving a ^{15}N (CANCO) evolution time of 4.8 ms and ^{13}C (NCACX) evolution time of 2.4 ms. 512 transients were co-added for each t1 and t2 increment. A recycle delay of 2 s was used.

The ^{13}C-dimension was referenced externally with adamantane at 40.48 ppm and the ^{15}N dimension was referenced indirectly from the ^{13}C-dimension. All spectra were processed with NMRPipe (Delaglio et al. 1995) and analyzed with Sparky (Goddard and Kneller 2008). A Lorentz-to-Gauss apodization of 60–80 Hz was used in the direct and indirect dimensions. The matrix size before Fourier transformation was 16,384 × 512 × 512.

Structure calculations

As the experiments were performed in lipid bicelles with the bicelle-director perpendicular to the external magnetic field, the ^{15}N average isotropic chemical shift of 120 ppm and ^{1}H isotropic chemical shift of 8.1 ppm were subtracted from each observed anisotropic chemical shift and scaled by 2.5 to obtain the input restraints for structure calculations. Observed dipolar couplings were also scaled by 2.5 to obtain the necessary restraints. This factor of 2.5 is a combination of the scaling of anisotropic parameters by 2 in the parallel orientation and a scaling factor of 1.25 to account for bicelle motions (Nevzorov 2011). Restraints were incorporated with an associated error of ±5 ppm for ^{15}N chemical shifts, ±1.5 ppm for ^{1}H chemical shifts and ±0.5 kHz for dipolar couplings. Dihedral angle restraints from MAS-ssNMR were calculated using the isotropic chemical shifts of Cα, Cβ, C′ and N (amide) atoms as an input for TALOS+ (Shen et al. 2009) and implemented with an error of ±30°.

All oriented ssNMR restraints (anisotropic chemical shifts for amide ^{15}N and amide ^{1}H and ^{15}N-^{1}H dipolar couplings) and MAS-ssNMR restraints (dihedral restraints from TALOS) were combined in a single energy function along with potentials corresponding to standard peptide geometry ($E_{chem} = E_{bond} + E_{angle} + E_{improper} + E_{vdW}$) (Schwieters et al. 2003). In addition, hydrogen bonds between the carbonyl oxygen and amide proton of {i} and {i + 4} residues were implemented for the transmembrane segment. Orientation restraints were implemented with flat-well harmonic potentials using csaPot and rdcPot modules from XPLOR-NIH (version 2.29). These inbuilt C++ based modules allow for a faster calculation of structure than the PYTHON based modules (Bertram et al. 2000) we previously used (Shi et al. 2009b) for the structure determination. The ^{15}N tensor was defined with the requisite parameters in XPLOR-NIH with the following traceless CSA tensor components: $\sigma 11 = 55.3$ ppm, $\sigma 22 = -97.6$ ppm, $\sigma 33 = 43.3$ ppm, $\beta = -17°$ and $\gamma = 0°$. Similarly, ^{1}H

traceless tensor components were defined with $\sigma 11 = 6.3$ ppm, $\sigma 22 = 1.3$ ppm, $\sigma 33 = -7.6$ ppm, $\beta = 97°$ and $\gamma = 0°$ (Yao et al. 2010).

The hybrid energy function ($E_{O\text{-}ssNMR}$, $E_{MAS\text{-}ssNMR}$ and E_{chem}) was minimized using a simulated annealing protocol in the torsion angle space. Starting from an extended conformation of SLN, we carried out simulated annealing after an initial equilibration step at 6,000 K for 10 ps. The temperature was decreased in steps of 5 K with a 0.5 ps time step to reach a final temperature of 10 K. A knowledge based E_z-potential (Senes et al. 2007) was implemented as this stage to insert SLN into a virtual membrane bilayer. The structure was then equilibrated at 10 K for 20 ps and subjected to Powell Minimization in Cartesian space. Of 200 structures generated, 10 lowest energy structures were selected for simulated annealing in the Cartesian space to relax local geometries. ^{1}H-CSA restraints were included at this stage. After a 10 ps equilibration at 300 K, the temperature was reduced to 5 K in steps of 2.5 K, with 0.5 ps simulation at each step. E_z-potential was again implemented and a final equilibration at 5 K for 20 ps followed by Powell minimization was carried out to give the final structure. One hundred structures were generated and the ten lowest energy conformers were selected for further analysis. The convergence of the lowest energy structures was determined by aligning the projections of each of the structures on the XY plane (Shi et al. 2009b). The RMSD of each conformer from the average structure was calculated without further manipulation of the coordinates in order to maintain the topology calculated from anisotropic NMR parameters. The tilt angle (with respect to the bilayer normal) and rotation angle (with respect to the Cα atom of residue R6) were calculated by aligning a model 20-residue alpha helix with the residues 14–28. Quality of the final structure ensemble was validated by ProCheck (Laskowski et al. 1996) and MolProbity (Davis et al. 2007), as well as the convergence of R-values for individual orientation restraints.

Results

Magnetically aligned bicelle samples give spectra with a sensitivity and resolution higher than mechanically aligned samples. The latter combined with the ease of sample preparation, better hydration, pH control and sample stability makes bicelles an excellent membrane mimetic for O-ssNMR experiments (Veglia et al. 2012; Dürr et al. 2012). This allows highly sensitive samples to be prepared for 3-dimensional spectroscopy. Fig S1 shows a typical 1D spectrum after initial optimization of CP conditions. For SLN, these preparations give 2D SLF spectra with remarkable resolution and a distinct PISA-wheel pattern (Page and Cross 2008; Mote et al. 2011). All these improvements make it possible to acquire 3D experiments with the sensitivity enhancement pulse sequences. Figure 2 shows strip plots from the 3D-SE-PISEMAI-HETCOR experiment. All of the resonances belonging to the transmembrane domain of SLN are present and well resolved, with characteristic oscillatory patterns (Mesleh et al. 2002; Mascioni and Veglia 2003) evident for the chemical shifts and the dipolar couplings. We have previously assigned the 2D SE-PISEMA spectrum for SLN in these lipids using a 3D-SE-PISEMA-PDSD experiment that allowed for a sequential assignment using ^{15}N-^{15}N correlations established by proton driven spin diffusion (Mote et al. 2011). This allowed a straightforward transfer of the assignment to the resonances observed in the 3D SE-PISEMAI-HETCOR experiment. The high quality of the spectrum, with linewidths for ^{15}N-CS of ~150 Hz, ^{1}H-CS of ~800–1,000 Hz and the ^{15}N-^{1}H DC of ~100 Hz allowed us to obtain the set of orientation restraints that completely describe the backbone topology.

For a rapid screen to determine the relative dispersion attainable in each dimension, as well as optimizing mixing times for the DARR element (Takegoshi et al. 2001) in the pulse sequence, we used the 2D-MEIOSIS experiment. Figure 3 shows a variant of this experiment, i.e. MEIOSIS-(DARR-CA(N)CO-NCO-N(CA)CX), in which the four 2D spectra are obtained simultaneously within a single experiment. Although several peaks are resolved and residue type assignments are easily obtained from these experiments, they give only an ambiguous assignment. The comparatively low resolution in the 2D spectra is a direct result of fast T2 relaxation, which is also observed for other small membrane embedded proteins (Su et al. 2011), and underscores the importance of 3D experiments to assign these proteins. In the N(CA)CX obtained at 10 ms mixing time, it is possible to identify several intense correlations, indicating that the mixing period is sufficient to transfer the polarization from the backbone to the side chains. At a 10 ms mixing time, the N(CA)CX spectrum shows several

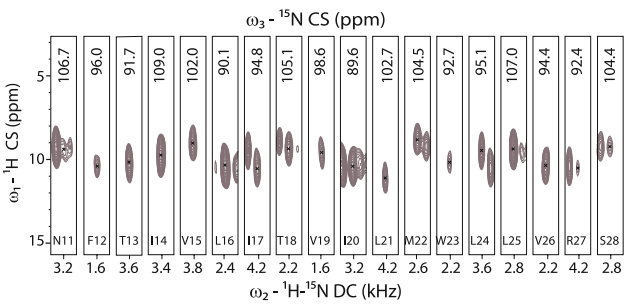

Fig. 2 Strip plot of the 3D-SE-PISEMAI-HETCOR spectrum. All resonances from N11 to S28 are completely resolved and assigned based on our previous assignment for the 2D spectrum. Average signal is 55σ (range of 24σ–124σ). Spectrum is plotted starting at 18σ with contours progressing by factor of 1.2

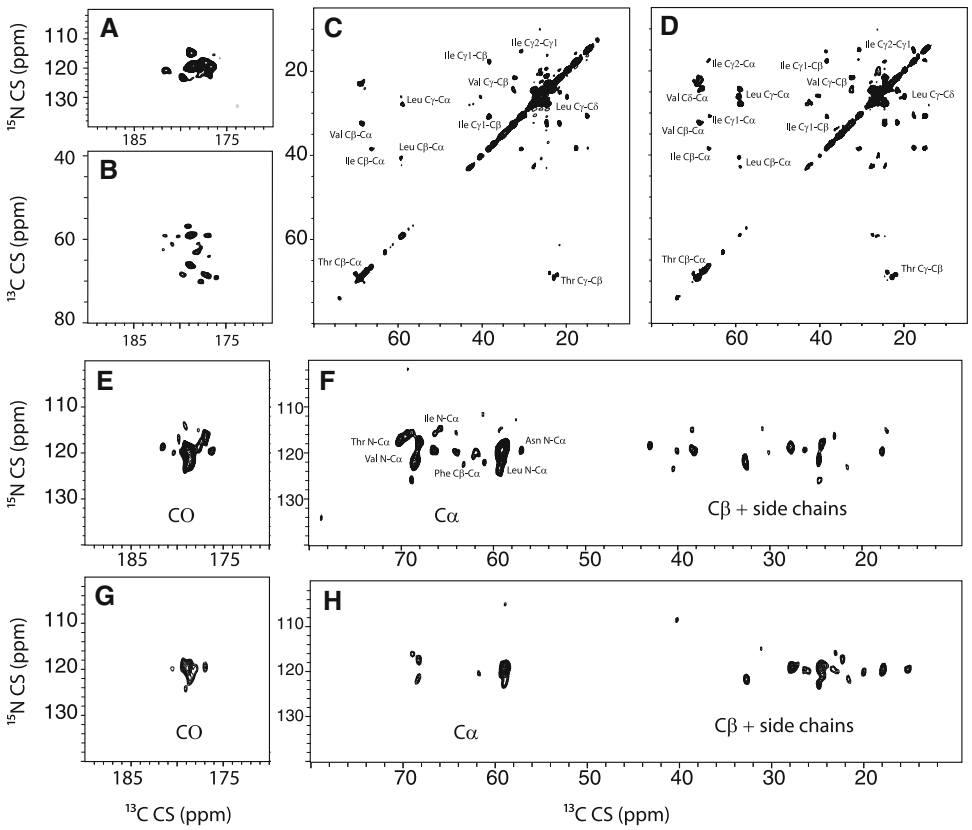

Fig. 3 Spectra obtained with MEIOSIS-(DARR/CA(N)CO/N(CA)CX/NCO) pulse sequence **a** NCO correlation, **b** CA(N)CO correlation. **c** ^{13}C-^{13}C DARR correlation with 10 ms mixing time, **d** ^{13}C-^{13}C DARR correlation with 50 ms mixing time, **e**, **f** N(CA)CX correlations with 10 ms mixing time and **g**, **h** N(CA)CX correlation with 50 ms mixing time. **c** and **d** are plotted starting at 7σ and contours progressing by a factor of 1.1. All other spectra are plotted starting at 6σ with contours progressing by a factor of 1.1

Cβ and C′ resonances. At a 50 ms mixing time, the Cβ and possibly the other side chain peaks increase in intensity at the expense of both C′ and Cα. Our assignment strategy relies on obtaining information on residue type using statistically predicted chemical shifts and connecting these residues via a 'backbone-walk'. Based on this screening, we concluded that the DUMAS-CANCO/NCACX pulse sequence with a 10 ms mixing time during the DARR transfer in NCACX is optimal for assigning SLN, as it would give information on the residue type in the NCACX spectrum and also allow a simultaneous main-chain walk via the common carbonyl resonance of the {i} and {i + 1} spin systems. A mixing time of 10 ms was deemed optimal as longer mixing times decreased the intensity of the C′ resonances. After assignment of a majority of residue types in the transmembrane segment based on the statistical Cα and Cβ chemical shifts obtained from the 2D and the 3D spectra, we sequentially assigned the transmembrane segment from residue E7 to V26 by the classical 'main chain walk', aligning the carbonyl chemical shifts for {i} and {i + 1} residues (Fig. 4). This assignment was aided by relatively high sequence variation in the SLN transmembrane domain, which has threonine, methionine and tryptophan residues in addition to the hydrophobic leucine, isoleucine and valine residues frequently found in TM domains. The leucine region of the spectrum (~58 ppm) suffers from severe overlap of resonance. However, with resolution in the carbonyl region of the spectrum, we were also able to assign these residues. Residues N4-R6 which are known to undergo conformational dynamics, were not assigned, possibly due to inefficient cross-polarization for these residues. The terminal residues M1-I3 and Y31 were assigned in a refocused-INEPT experiment at 298.15 K (Supplementary Fig 2).

Figure 5a shows the ensembles of the SLN conformers obtained. The high precision of the ensemble (backbone, incl. H^N + Cβ RMSD ~0.44 Å) is also reflected in low energies for all structural restraints. The global as well as the individual R-values for all orientation restraints are converged below 1 (Fig. 5e–g), indicating a good agreement between the calculated structures and the experimental O-ssNMR data. Table 1 summarizes the structural statistics for these calculations. The hybrid NMR ensemble shows disordered N- and C-termini in agreement with the solution NMR ensemble obtained in DPC micelles (Mascioni et al. 2002; Buffy et al. 2006a). The resonances corresponding to residues 29–31 detected by SE-PISEMA experiments in aligned bicelles show dipolar couplings that are scaled down by the substantial motions in these segments and hence were not included in the final structure calculations. For the most structured residues (Residues 6–28), hybrid NMR ensemble shows a higher precision than

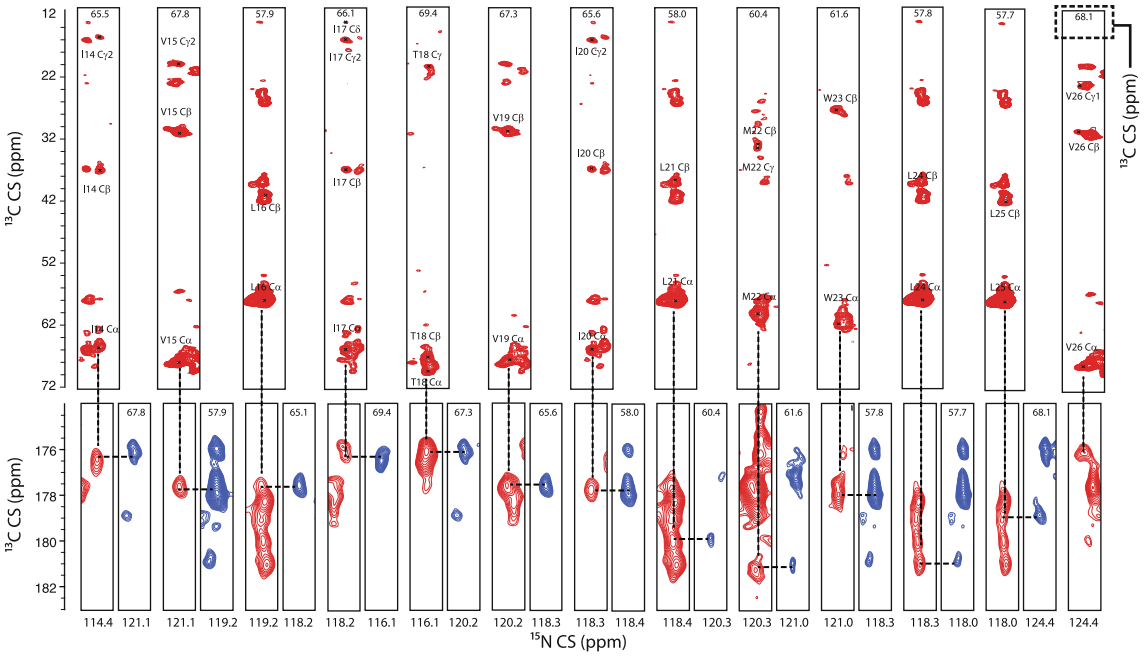

Fig. 4 Strip plots from the 3D-DUMAS-NCACX (*red*)/CANCO (*blue*) experiment. NCACX spectrum is plotted starting at 12σ (Cα-Cβ region) and 8.5σ (C′ region) and contours progressing by a factor of 1.1. Average signal per residue for NCACX is 28σ (Cα-Cβ region, range 12σ–63σ) and 15σ (carbonyl region, range 9σ–25σ). CANCO spectrum is plotted starting at 6σ and contours progressing by a factor 1.1. The average signal for per residue is 10σ (range 7σ–20σ). The average linewidth in each spectrum is ∼1.1 ppm for ^{13}Cα (indirect dimension), 1.0 ppm ^{13}C′ (direct dimension) and 2.5 ppm for ^{15}N (indirect dimension)

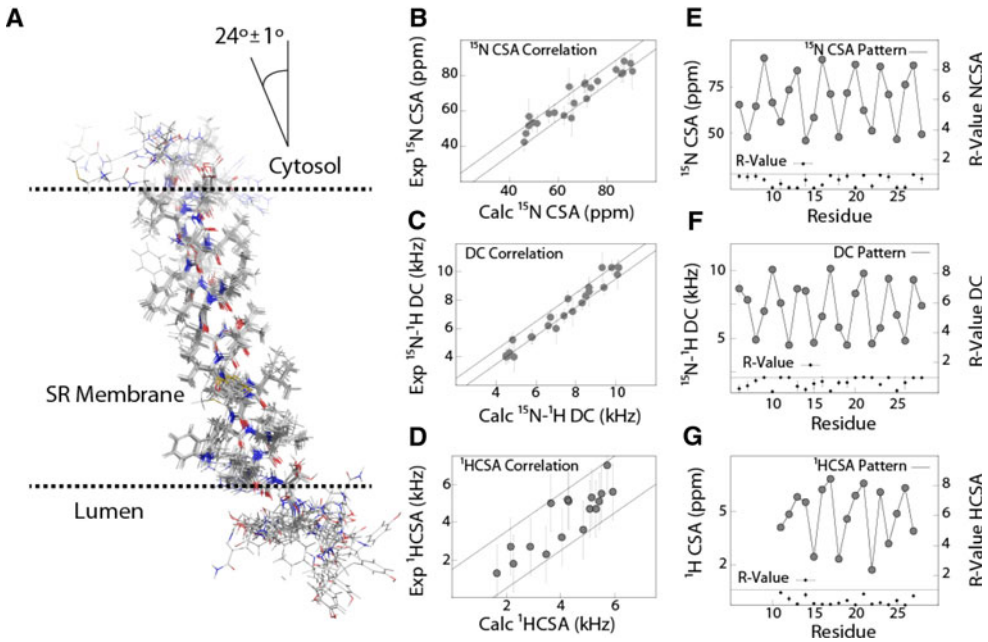

Fig. 5 **a** Structure ensemble obtained for SLN from the hybrid MAS/O-ssNMR structure calculations (10 lowest energy structures). **b–d** Correlation of experimental O-ssNMR restraints with the back-calculated restraints. **e–f** Oscillation patterns for all orientation restraints and the R-values of back-calculated restraints

the corresponding solution NMR ensemble (PDB Code: 1JDM). The topology is converged to a well-defined minimum in the conformational space. The tilt angle for SLN with respect to the bilayer normal was found to be 24° ± 1° and the rotation angle was 57° ± 5°. The indole ring of W23 is oriented with its plane parallel to the bilayer normal, with the N–H bond vector oriented in the direction of the C-terminal bilayer interface, possibly making contact with the phosphate head groups. Along with W23, the conserved residues R6, located near the cytosolic N-terminus, and R27, near the lumenal C-terminus, anchor SLN to the lipid membrane, modulating the tilt and rotation angles which

Table 1 Summary of structure ensemble statistics (10 structures)

RMSD from MAS NMR Restraints	
NH-C(O) hydrogen bond (Å)	0.052 ± 0.004
Dihedral Angles (TALOS)	0.000 ± 0.000
PISEMA R-factors	
^{15}N CSA	0.5 ± 0.4
^{15}N-^{1}H DC	0.7 ± 0.3
^{1}H CSA	0.3 ± 0.3
RMSD from idealized covalent geometry	
Bond (Å)	0.004 ± 0.000
Angle (°)	0.60 ± 0.01
Improper angle (°)	0.13 ± 0.01
Measure of structure quality (%)	
Most favored region	99 ± 1
Additionally allowed region	1 ± 1
Generously allowed region	0
Disallowed region	0
MolProbity® Score	98 ± 2 percentile
Precision of structures (RMSD for atoms $N^H + H^N + C' + O + C\alpha + C\beta$) (Å)	
Domain Ib + II (Res 6–28)	0.43
Domain Ib (Res 6–13)	0.44
Domain II (Res 14–28)	0.40
Protein topology	
Tilt angle (Res 6–28) (°)	24 ± 1
Rotation angle (from R6-Cα) (°)	55 ± 5
Depth of insertion (R6-Cα) (Å)	16.1 ± 0.2

seem to be only minimally affected in the different membrane mimetic systems (Mote et al. 2011). The NMR structural ensembles determined by the hybrid method are in good agreement with molecular dynamics simulations (Shi et al. 2009a) which show a similar orientation of the indole side chain of W23, and a previous oriented solid state NMR study (Buffy et al. 2006b) carried out mechanically aligned DOPC/DOPE bilayers, which shows a similar the tilt angle of $\sim 23°$ with respect to the bilayer.

Discussion

While multidimensional MAS-ssNMR techniques are mature for structure determination of large systems, their application to membrane proteins is limited by the sensitivity and resolution that can be attained in these systems. Obtaining complete resolution is often not possible without 3D experiments, which take a long time due to the poor sensitivity of these systems. The DUMAS strategy allowed us to substantially reduce experimental time as compared with traditional MAS-ssNMR pulse sequences. The initial experiments with MEIOSIS allowed the determination of parameters, such as the appropriate mixing time, that were important to set up the 3-dimensional experiments for assignments. These initial experiments also allowed us to determine the best possible experimental approach to assign the protein based on relative resolution attainable in each dimension. The DUMAS-CANCO/NCACX experiment allowed us to assign a majority of the protein sequentially as the experiment combines the complementary pulse sequence into a single experiment. Moreover, the simultaneous acquisition of both the experiments allowed the data to be fairly compared without the need for concern regarding sample or instrumental stability.

Compared to MAS-ssNMR, multidimensional O-ssNMR spectroscopy is still in its infancy, in spite of the fact that the number of membrane protein structures being solved by this technique is greater. Sensitivity gains obtained from the 3D-SE-PISEMAI-HETCOR are a substantial leap forward in obtaining complete resolution for these studies. It must be noted here that the resolution of the structure depends primarily on the O-ssNMR data, as the secondary structure obtained from MAS-ssNMR experiments contains no information on the topological parameters of tilt and rotation angle. As such, the O-ssNMR experiments described herein are indispensable in order to characterize the structure of membrane proteins precisely. TALOS based dihedral angle restraints obtained from MAS-ssNMR are a perfect complement to these orientation restraints from O-ssNMR and help convergence of the structure ensemble in spite of inherent degeneracy in the observed values of dipolar couplings and anisotropic chemical shifts.

In the past these MAS-ssNMR and O-ssNMR techniques were thought to be mutually exclusive and most researchers used either MAS or O-ssNMR for de novo structure determination. Recent developments of structural biology emphasize the use of multiple techniques to substantiate biological and structural data (Traaseth et al. 2007; Shi et al. 2011b). In this spirit, we combined MAS-ssNMR and O-ssNMR restraints into a unique refinement protocol. The idea to combine these techniques is similar to solution NMR, where distance and torsion angle restraints are energy minimized together with residual dipolar couplings to obtain high-resolution structures and reciprocal orientations of protein domains. While some concerns can be raised regarding the compatibility of solution NMR restraints in micelles, which can also serve as complements to O-ssNMR restraints, the agreement between MAS and O-ssNMR data stems from the similarity between the two membrane mimicking environments.

Conclusions

We show here that the complete set of high resolution restraints for both MAS-ssNMR and O-ssNMR can be

conveniently obtained for membrane proteins using POE for both oriented and MAS-ssNMR spectroscopy. The combination of structural and topological restraints from these techniques into a hybrid NMR calculation approach makes it possible to determine the high resolution structure and topology of membrane proteins. Although we anticipate that POE experiments will have the biggest impact on data acquisition of membrane proteins, they are universally applicable to other biomacromolecular systems.

Acknowledgments We thank Dr. Martin Gustavsson and Dr. Vitaly Vostrikov for helpful discussions. This work is supported by the National Institute of Health (GM64742 to G.V.). The experiments were carried out at the University Of Minnesota NMR Center.

References

Asami S, Szekely K, Schanda P, Meier BH, Reif B (2012) Optimal degree of protonation for ^{1}H detection of aliphatic sites in randomly deuterated proteins as a function of the MAS frequency. J Biomol NMR 54:155–168

Bertram R, Quine JR, Chapman MS, Cross TA (2000) Atomic refinement using orientational restraints from solid-state NMR. J Magn Reson 147:9–16

Buck B, Zamoon J, Kirby TL, DeSilva TM, Karim C, Thomas D, Veglia G (2003) Overexpression, purification, and characterization of recombinant Ca-ATPase regulators for high-resolution solution and solid-state NMR studies. Protein Expr Purif 30:253–261

Buffy JJ, Buck-Koehntop BA, Porcelli F, Traaseth NJ, Thomas DD, Veglia G (2006a) Defining the intramembrane binding mechanism of sarcolipin to calcium ATPase using solution NMR spectroscopy. J Mol Biol 358:420–429

Buffy JJ, Traaseth NJ, Mascioni A, Gor'kov PL, Chekmenev EY, Brey WW, Veglia G (2006b) Two-dimensional solid-state NMR reveals two topologies of sarcolipin in oriented lipid bilayers. Biochemistry 45:10939–10946

Cady SD, Mishanina TV, Hong M (2009) Structure of amantadine-bound M2 transmembrane peptide of influenza A in lipid bilayers from magic-angle-spinning solid-state NMR: the role of Ser31 in amantadine binding. J Mol Biol 385:1127–1141

Canlas CG, Ma D, Tang P, Xu Y (2008) Residual dipolar coupling measurements of transmembrane proteins using aligned low-q bicelles and high-resolution magic angle spinning NMR spectroscopy. J Am Chem Soc 130:13294–13300

Castellani F, van Rossum B, Diehl A, Schubert M, Rehbein K, Oschkinat H (2002) Structure of a protein determined by solid-state magic-angle-spinning NMR spectroscopy. Nature 420: 98–102

Das BB, Nothnagel HJ, Lu GJ, Son WS, Tian Y, Marassi FM, Opella SJ (2012) Structure determination of a membrane protein in proteoliposomes. J Am Chem Soc 134:2047–2056

Davis IW, Leaver-Fay A, Chen VB, Block JN, Kapral GJ, Wang X, Murray LW et al (2007) MolProbity: all-atom contacts and structure validation for proteins and nucleic acids. Nucleic Acids Res 35:W375–W383

Delaglio F, Grzesiek S, Vuister GW, Zhu G, Pfeifer J, Bax A (1995) NMRPipe: a multidimensional spectral processing system based on UNIX pipes. J Biomol NMR 6:277–293

Demers JP, Chevelkov V, Lange A (2011) Progress in correlation spectroscopy at ultra-fast magic-angle spinning: basic building blocks and complex experiments for the study of protein structure and dynamics. Solid State Nucl Magn Reson 40: 101–113

Dürr UHN, Gildenberg M, Ramamoorthy A (2012) The magic of bicelles lights up membrane protein structure. Chem Rev 112:6054–6074

Dvinskikh SV, Yamamoto K, Ramamoorthy A (2006) Heteronuclear isotropic mixing separated local field NMR spectroscopy. J Chem Phys 125:034507–034519

Giraud N, Blackledge M, Goldman M, Böckmann A, Lesage A, Penin F, Emsley L (2005) Quantitative analysis of backbone dynamics in a crystalline protein from nitrogen-15 spin-lattice relaxation. J Am Chem Soc 127:18190–18201

Goddard TG, Kneller DG (2008) SPARKY 3.114. University of California, San Francisco

Gopinath T, Veglia G (2009) Sensitivity enhancement in static solid-state NMR experiments via single- and multiple-quantum dipolar coherences. J Am Chem Soc 131:5754–5756

Gopinath T, Veglia G (2010) Improved resolution in dipolar NMR spectra using constant time evolution PISEMA experiment. Chem Phys Lett 494:104–110

Gopinath T, Veglia G (2012a) Dual acquisition magic-angle spinning solid-state NMR-spectroscopy: simultaneous acquisition of multidimensional spectra of biomacromolecules. Angew Chem Int Ed 51:2731–2735

Gopinath T, Veglia G (2012b) 3D DUMAS: simultaneous acquisition of three-dimensional magic angle spinning solid-state NMR experiments of proteins. J Magn Reson 220:79–84

Gopinath T, Veglia G (2013) Orphan spin operators enable the acquisition of multiple 2D and 3D magic angle spinning solid-state NMR spectra. J Chem Phys 138:184201

Gopinath T, Traaseth NJ, Mote K, Veglia G (2010a) Sensitivity enhanced heteronuclear correlation spectroscopy in multidimensional solid-state NMR of oriented systems via chemical shift coherences. J Am Chem Soc 132:5357–5363

Gopinath T, Verardi R, Traaseth NJ, Veglia G (2010b) Sensitivity enhancement of separated local field experiments: application to membrane proteins. J Phys Chem B 114:5089–5095

Gopinath T, Mote KR, Veglia G (2011) Proton evolved local field solid-state nuclear magnetic resonance using Hadamard encoding: theory and application to membrane proteins. J Chem Phys 135:074503

Gor'kov PL, Chekmenev EY, Li C, Cotten M, Buffy JJ, Traaseth NJ, Veglia G, Brey WW (2007) Using low-E resonators to reduce RF heating in biological samples for static solid-state NMR up to 900 MHz. J Magn Reson 185:77–93

Hall DA, Maus DC, Gerfen GJ, Inati SJ, Becerra LR, Dahlquist FW, Griffin RG (1997) Polarization-enhanced NMR spectroscopy of biomolecules in frozen solution. Science 276:930–932

Hu F, Luo W, Hong M (2010) Mechanisms of proton conduction and gating in influenza M2 proton channels from solid-state NMR. Science 330:505–508

Ketchem RR, Hu W, Cross TA (1993) High-resolution conformation of gramicidin A in a lipid bilayer by solid-state NMR. Science 261:1457–1460

Knight MJ, Pell AJ, Bertini I, Felli IC, Gonnelli L, Pierattelli R, Herrmann T, Emsley L, Pintacuda G (2012) Structure and backbone dynamics of a microcrystalline metalloprotein by solid-state NMR. Proc Natl Acad Sci USA 109:11095–11100

Laskowski RA, Rullmannn JA, MacArthur MW, Kaptein R, Thornton JM (1996) AQUA and PROCHECK-NMR: programs for checking the quality of protein structures solved by NMR. J Biomol NMR 8:477–486

Linser R, Bardiaux B, Higman V, Fink U, Reif B (2011) Structure calculation from unambiguous long-range amide and methyl ^{1}H-^{1}H distance restraints for a microcrystalline protein with MAS solid-state NMR spectroscopy. J Am Chem Soc 133:5905–5912

Lopez JJ, Kaiser C, Asami S, Glaubitz C (2009) Higher sensitivity through selective ^{13}C excitation in solid-state NMR spectroscopy. J Am Chem Soc 131:15970–15971

Loquet A, Lv G, Giller K, Becker S, Lange A (2011) 13C spin dilution for simplified and complete solid-state NMR resonance assignment of insoluble biological assemblies. J Am Chem Soc 133:4722–4725

Loquet A, Sgourakis NG, Gupta R, Giller K, Riedel D, Goosmann C, Griesinger C et al (2012) Atomic model of the type III secretion system needle. Nature 486:276–279

Marchetti A, Jehle S, Felletti M, Knight MJ, Wang Y, Xu ZQ, Park AY et al (2012) Backbone assignment of fully protonated solid proteins by ^{1}H detection and ultrafast magic-angle-spinning NMR spectroscopy. Angew Chem Int Ed 51:10756–10759

Mascioni A, Veglia G (2003) Theorotical analysis of residual dipolar couplings in regular secondary structure of proteins. J Am Chem Soc 125:12520–12526

Mascioni A, Karim C, Barany G, Thomas DD, Veglia G (2002) Structure and orientation of sarcolipin in lipid environments. Biochemistry 41:475–482

Maudsley AA, Ernst RR (1977) Indirect detection of magnetic resonance by heteronuclear two-dimensional spectroscopy. Chem Phys Lett 50:368–372

Mesleh MF, Veglia G, DeSilva TM, Marassi FM, Opella SJ (2002) Dipolar waves as NMR maps of protein structure. J Am Chem Soc 124:4206–4207

Miao Y, Qin H, Fu R, Sharma M, Can TV, Hung I, Luca S, Gor'kov PL, Brey WW, Cross TA (2012) M2 proton channel structural validation from full-length protein samples in synthetic bilayers and *E. coli* membranes. Angew Chem Int Ed 51:8383–8386

Mote KR, Gopinath T, Traaseth NJ, Kitchen J, Gor'kov PL, Brey WW, Veglia G (2011) Multidimensional oriented solid-state NMR experiments enable the sequential assignment of uniformly ^{15}N labeled integral membrane proteins in magnetically aligned lipid bilayers. J Biomol NMR 51:339–346

Nevzorov AA (2011) Orientational and motional narrowing of solid-state NMR lineshapes of uniaxially aligned membrane proteins. J Phys Chem B 115:15406–15414

Nevzorov AA, Opella SJ (2003) A "magic sandwich" pulse sequence with reduced offset dependence for high-resolution separated local field spectroscopy. J Magn Reson 164:182–186

Nielsen AB, Székely K, Gath J, Ernst M, Nielsen NC, Meier BH (2012) Simultaneous acquisition of PAR and PAIN spectra. J Biomol NMR 52:283–288

Nieuwkoop AJ, Rienstra CM (2010) Supramolecular protein structure determination by site-specific long-range intermolecular solid state NMR spectroscopy. J Am Chem Soc 132:7570–7571

Odermatt A, Becker S, Khanna VK, Kurzydlowski K, Leisner E, Pette D, MacLennan DH (1998) Sarcolipin regulates the activity of SERCA1, the fast-twitch skeletal muscle sarcoplasmic reticulum Ca^{2+}-ATPase. J Biol Chem 273:12360–12369

Page RC, Cross TA (2008) Transmembrane helix uniformity examined by spectral mapping of torsion angles. Structure 16:787–797

Park SH, Marassi FM, Black D, Opella SJ (2010) Structure and dynamics of the membrane-bound form of Pf1 coat protein: implications of structural rearrangement for virus assembly. Biophys J 99:1465–1474

Park SH, Das BB, Casagrande F, Tian Y, Nothnagel HJ, Chu M, Kiefer H et al (2012) Structure of the chemokine receptor CXCR1 in phospholipid bilayers. Nature 491:779–783

Reif B (2012) Ultra-high resolution in MAS solid-state NMR of perdeuterated proteins: implications for structure and dynamics. J Magn Reson 216:1–12

Reif B, Jaroniec CP, Rienstra CM, Hohwy M, Griffin RG (2001) ^{1}H-^{1}H MAS correlation spectroscopy and distance measurements in a deuterated peptide. J Magn Reson 151:320–327

Renault M, Pawsey S, Bos MP, Koers EJ, Nand D, Tommassen-van Boxtel R, Rosay M, Tommassen J, Maas WE, Baldus M (2012a) Solid-state NMR spectroscopy on cellular preparations enhanced by dynamic nuclear polarization. Angew Chem Int Ed 51: 2998–3001

Renault M, Tommassen-van Boxtel R, Bos MP, Post JA, Tommassen J, Baldus M (2012b) Cellular solid-state nuclear magnetic resonance spectroscopy. Proc Natl Acad Sci USA 109:4863–4868

Schmidt-Rohr K, Nanz D, Emsley L, Pines A (1994) NMR measurement of resolved heteronuclear dipole couplings in liquid crystals and lipids. J Phys Chem 98:6668–6670

Schwieters CD, Kuszewski JJ, Tjandra N, Clore GM (2003) The Xplor-NIH NMR molecular structure determination package. J Magn Reson 160:65–73

Senes A, Chadi DC, Law PB, Walters RF, Nanda V, Degrado WF (2007) E(z), a depth-dependent potential for assessing the energies of insertion of amino acid side-chains into membranes: derivation and applications to determining the orientation of transmembrane and interfacial helices. J Mol Biol 366:436–448

Sharma M, Yi M, Dong H, Qin H, Peterson E, Busath DD, Zhou HX, Cross TA (2010) Insight into the mechanism of the influenza A proton channel from a structure in a lipid bilayer. Science 330:509–512

Shen Y, Delaglio F, Cornilescu G, Bax A (2009) TALOS +: a hybrid method for predicting protein backbone torsion angles from NMR chemical shifts. J Biomol NMR 44:213–223

Shi L, Cembran A, Gao J, Veglia G (2009a) Tilt and azimuthal angles of a transmembrane peptide: a comparison between molecular dynamics calculations and solid-state NMR data of sarcolipin in lipid membranes. Biophys J 96:3648–3662

Shi L, Traaseth NJ, Verardi R, Cembran A, Gao J, Veglia G (2009b) A refinement protocol to determine structure, topology, and depth of insertion of membrane proteins using hybrid solution and solid-state NMR restraints. J Biomol NMR 44:195–205

Shi L, Kawamura I, Jung K-H, Brown LS, Ladizhansky V (2011a) Conformation of a seven-helical transmembrane photosensor in the lipid environment. Angew Chem Int Ed 50:1302–1305

Shi L, Traaseth NJ, Verardi R, Gustavsson M, Gao J, Veglia G (2011b) Paramagnetic-based NMR restraints lift residual dipolar coupling degeneracy in multidomain detergent-solubilized membrane proteins. J Am Chem Soc 133:2232–2241

Sperling LJ, Berthold DA, Sasser TL, Jeisy-Scott V, Rienstra CM (2010) Assignment strategies for large proteins by magic-angle spinning NMR: the 21-kDa disulfide-bond-forming enzyme DsbA. J Mol Biol 399:268–282

Su Y, Waring AJ, Ruchala P, Hong M (2011) Structures of beta-hairpin antimicrobial protegrin peptides in lipopolysaccharide membranes: mechanism of gram selectivity obtained from solid-state nuclear magnetic resonance. Biochemistry 50:2072–2083

Takegoshi K, Nakamura S, Terao T (2001) Dipolar-assisted rotational resonance in magic-angle spinning NMR. Chem Phys Lett 344:631–637

Tamm LK (2005) Protein lipid interactions: from membrane domains to cellular networks. Wiley-VCH Verlag GmbH & Co. KGaA, Weinheim, Germany

Tang M, Sperling LJ, Berthold DA, Schwieters CD, Nesbitt AE, Nieuwkoop AJ, Gennis RB, Rienstra CM (2011) High-resolution membrane protein structure by joint calculations with solid-state NMR and X-ray experimental data. J Biomol NMR 51:227–233

Traaseth NJ, Verardi R, Torgersen KD, Karim CB, Thomas DD, Veglia G (2007) Spectroscopic validation of the pentameric structure of phospholamban. Proc Natl Acad Sci USA 104:14676–14681

Traaseth NJ, Ha KN, Verardi R, Shi L, Buffy JJ, Masterson LR, Veglia G (2008) Structural and dynamic basis of phospholamban and sarcolipin inhibition of Ca^{2+}-ATPase. Biochemistry 47:3–13

Traaseth NJ, Shi L, Verardi R, Mullen DG, Barany G, Veglia G (2009) Structure and topology of monomeric phospholamban in lipid membranes determined by a hybrid solution and solid-state NMR approach. Proc Natl Acad Sci USA 106:10165–10170

Veglia G, Ha KN, Shi L, Verardi R, Traaseth NJ (2010) What can we learn from a small regulatory membrane protein? Methods Mol Biol 654:303–319

Veglia G, Traaseth NJ, Shi L, Verardi R, Gopinath T, Gustavsson M (2012) The hybrid solution/solid-state NMR method for membrane protein structure determination. In: Egelman EH (ed) Comprehensive biophysics. Elsevier, Amsterdam, pp 182–198

Verardi R, Shi L, Traaseth NJ, Walsh N, Veglia G (2011) Structural topology of phospholamban pentamer in lipid bilayers by a hybrid solution and solid-state NMR method. Proc Natl Acad Sci USA 108:9101–9106

White SH (2009) Biophysical dissection of membrane proteins. Nature 459:344–346

Wu CH, Ramamoorthy A, Opella SJ (1994) High-resolution heteronuclear dipolar solid-state NMR spectroscopy. J Magn Reson A 109:270–272

Wylie BJ, Sperling LJ, Nieuwkoop AJ, Franks WT, Oldfield E, Rienstra CM (2011) Ultrahigh resolution protein structures using NMR chemical shift tensors. Proc Natl Acad Sci USA 108: 16974–16979

Yao L, Grishaev A, Cornilescu G, Bax A (2010) The impact of hydrogen bonding on amide ^{1}H chemical shift anisotropy studied by cross-correlated relaxation and liquid crystal NMR spectroscopy. J Am Chem Soc 132:10866–10875

Zhou DH, Nieuwkoop AJ, Berthold DA, Comellas G, Sperling LJ, Tang M, Shah GJ, Brea EJ, Lemkau LR, Rienstra CM (2012) Solid-state NMR analysis of membrane proteins and protein aggregates by proton detected spectroscopy. J Biomol NMR 54:291–305